**Articles in PresS. Am J Physiol Lung Cell Mol Physiol (March 27, 2015). doi:10.1152/ajplung.00291.2014**

# Attenuating endogenous Fgfr2b ligands during bleomycin-induced lung fibrosis does not compromise murine lung repair

BreAnne MacKenzie[1], Ingrid Henneke[1], Stefanie Hezel[1], Denise Al Alam[2], Elie El Agha[1], Cho-Ming Chao[1], Jennifer Quantius[1], Jochen Wilhelm[1], Matthew Jones[1], Kerstin Goth[1], Xiaokun Li[3], Werner Seeger[1], Melanie Königshoff[4], Susanne Herold[1], Albert A. Rizvanov[7], Andreas Günther[1,5,6], and Saverio Bellusci, [1,2,7,#]

[1]German Center for Lung Research, Excellence Cluster Cardio-Pulmonary System, Universities of Giessen and Marburg Lung Center, Giessen, Hessen, Germany.

[2]Developmental Biology Program, Division of Surgery, Saban Research Institute of Children's Hospital Los Angeles, University of Southern California Keck School of Medicine, Los Angeles, California

[3]School of Pharmacy, Wenzhou Medical College, China

[4]Comprehensive Pneumology Center, Ludwig Maximilians University, University Hospital Grosshadern, and Helmholtz Zentrum München, Munich, Bavaria, Germany.

[5]AGAPLESION Lung Clinic Waldhof-Elgershausen, Greifenstein, Germany

[6]Member of the German Center for Lung Research

[7]Institute of Fundamental Medicine and Biology, Kazan Federal University, 18 Kremlyovskaya Street, Kazan 420008, Russian Federation

[#] Corresponding author

Saverio.Bellusci@innere.med.uni-giessen.de

Abstract

Fibroblast growth factors (Fgfs) mediate organ repair. Lung epithelial cell overexpression of *Fgf10* post-bleomycin injury is both protective and therapeutic, characterized by increased survival and attenuated fibrosis. Exogenous administration of FGF7 (Palifermin) also showed prophylactic survival benefits in mice. The role of endogenous Fgfr2b ligands upon bleomycin-induced lung fibrosis is still elusive. This study reports the expression of endogenous Fgfr2b ligands, receptors and signaling targets in wild type mice following bleomycin lung injury. In addition, the impact of attenuating endogenous Fgfr2b-ligands following bleomycin-induced fibrosis was tested using a doxycycline (dox)-based inducible, soluble, dominant-negative form of the Fgfr2b receptor. Double transgenic (DTG) *Rosa26*$^{rtTA/+}$*;tet(O)solFgfr2b* mice were validated for the expression and activity of soluble Fgfr2b (failure to regenerate maxillary incisors, attenuated recombinant FGF7 signal in the lung). As previously reported, no defects in lung morphometry were detected in DTG (+dox) mice exposed from post-natal (PN) 1 through PN105. Female single transgenic (STG) and DTG mice were subjected to various levels of bleomycin injury (1.0, 2.0, and 3.0U/kg). Fgfr2b ligands were attenuated either throughout injury (d0-d11; d0-28) or during later stages (d6-d28 and d14-d28). No significant changes in survival, weight, lung function, confluent areas of fibrosis, or hydroxyproline deposition were detected in DTG mice. These results indicate that endogenous Fgfr2b ligands do not significantly protect against bleomycin injury, nor do they expedite the resolution of bleomycin lung induced injury in mice.

## Introduction

The interstitial lung disease, Idiopathic Pulmonary Fibrosis (IPF) occurs between the sixth and seventh decades of life at a rate of 2-4/10000 (21). 5-year survival rates approximate just 10-15% (21). The pathomechanism of IPF is not yet fully understood, however it is thought to occur as a result of chronic epithelial injury or stress, resulting in the accumulation of myofibroblasts which express high levels of extracellular matrix (19). Genetic manipulation of lung development pathways in the context of bleomycin-lung injury; including: Notch, transforming growth factor beta (Tgfβ), Bone morphogenetic protein (Bmp), Sonic hedgehog (Shh), fibroblast growth factors (Fgfs), epidermal growth factor (Egf), and wingless-type MMTV integration site family, (Wnt), combined with results based on studies using IPF patient materials have led to the development of potential therapeutic treatments for IPF (31, 38).

Fgf7 and Fgf10 signal in a paracrine fashion via epithelially-expressed Fgfr2b receptor (43). The signal results in a phosphorylation cascade, mediated by fibroblast growth factor receptor substrate (Frs2), which activates PI3k- and Mapk-signaling pathways and/or activation of phospholipase C gamma (Plc-γ). Depending on the cell type and context, Fgfr2b-signaling culminates in survival, growth and differentiation of epithelial cells. Fgf10/Fgfr2b signaling is critical for murine lung development while Fgf7 is dispensable (2, 16, 27). Fgfs have been reported to act upstream of Wnt-signaling (23). Interestingly, bleomycin-injured mice with epithelial specific deletion of ß-catenin-signaling, a downstream target of both Fgf- (23) and Wnt-signaling (26), suffered increased fibrosis (37). While Wnt-signaling was previously thought to play an exclusively pro-fibrotic role by mediating epithelial-to-mesenchymal transition (EMT), this report revealed the importance of ß-catenin-mediated protection of epithelial cells against bleomycin-injury.

In the bleomycin mouse model, past studies have focused primarily on the beneficial effect of prophylactic treatment with Palifermin, a pharmacological agent composed of a truncated form of keratinocyte growth factor (KGF), also known as, FGF7 (7, 36). While Palifermin demonstrated a protective, prophylactic effect, genetic *Fgf10* expression post-bleomycin injury (5) resulted in increased survival as well as prevention and accelerated resolution of lung fibrosis in mice. While current therapies target tyrosine kinases for the treatment of IPF (1), whether endogenous FGF-signaling plays a protective, pathogenic, or ambivalent role in IPF, is still unknown. Given the beneficial effects of exogenous Fgfr2b ligands on lung repair, the authors hypothesized that endogenous Fgfr2b ligands play a critical role in repair following bleomycin-injury. However, endogenous Fgfr2b ligands as well as Fgfr2b receptor expression, were decreased following bleomycin-injury in wild type mice. Thus unsurprisingly, attenuating endogenous Fgfr2b-ligands during bleomycin-induced lung injury did not lead to significantly increased fibrosis or decreased survival. In summary, although endogenous Fgfr2b ligand signaling failed to play a critical role in limiting fibrosis, these results do not

negate the potential benefit of exogenously stimulating developmental pathways to protect against lung fibrosis.

## Methods

### Animal Care

All experiments were performed in accordance with the National Institutes of Health Guidelines for the Use of Laboratory Animals. Animal experiments were approved by the Institutional Animal Care and Use Committee at Children's Hospital Los Angeles protocol 193-12 and the Federal Authorities for Animal Research of the Regierungspraesidium Giessen, Hessen, Germany protocols 72/2012 and 73/2012.

**Generation of Mice**

*CMV-Cre* mice (33) were crossed with *rtTA*$^{flox}$ mice (9) to generate mice expressing *rtTA* under the ubiquitous *Rosa26* promoter. This constitutive *Rosa26*$^{rtTA/+}$ mouse line was then crossed with the *tet(O)solFgfr2b/+* responder line to generate *Rosa26*$^{rtTA/+}$*;tet(O)sFgfr2b/+* double heterozygous animals, allowing ubiquitous expression of dominant-negative soluble Fgfr2b (28). All mice were generated on a CD1 mixed background. Attenuation of Fgfr2b ligand activity was achieved by administration of doxycycline-containing food; normal rodent diet with 0.0625% doxycycline (Harlan Teklad). Tet(O)Cre (B6.Cg-Tg(tetO-cre)1Jaw/J) (30) and *Tomato*$^{flox/flox}$ reporter mice (B6;129S6-Gt(ROSA)26Sortm9(CAG-tdTomato)Hze/J) (24) were purchased from Jackson lab. Mice were genotyped as described previously (3, 12, 34).

**Bleomycin administration**

10–14 week-old female mice were anaesthetized with a mixture of 0.6 µl/g Ketamine 10% (100 mg/ml) and 0.3 µl/g Dormitor 10% (0.5 mg/ml) dissolved in 0.7% saline. A microsprayer (PennCentury) was used to administer an intra-tracheal dose of either 0.7% saline or bleomycin (1.0–3.0U/kg) (Hexal, Germany or Sigma-Aldrich, USA). Weight, activity, respiration and temperature was monitored daily and mice were sacrificed if they showed a significant decline in health parameters.

**Lung compliance measurement**

Mice were deeply anaesthetized with a mixture of 1.2 µl/g Ketamine 10% (100 mg/mL, Bela Pharm, Germany), 0.6 µl/g Domitor 10% (0.5 mg/ml; Orion Finnland), 1:4 parts heparin, and dissolved in saline. Lung function was measured using the SCIREQ Flexi-Vent forced oscillation plethysmograph to give an overall readout of lung function. Mice were intubated trans-tracheally and ventilated at a rate of 150 breaths per minute with a positive end-expiratory pressure (PEEP) between 1 and 3 cmH2O. PEEP was calculated automatically by FlexiVent 7 software and dependent on the weight of the animal. After stable ventilation was achieved (spontaneous breathing ceased as the heart continued to beat) a 3 second, weight dependent, fixed volume waveform was initiated every 15 – 20 seconds, eight times. During this perturbation, "Snapshots" of respiratory compliance were taken and the average of eight measurements represented the value of one biological sample.

**Left lobe perfusion and isolation**

The left lobe was perfused from 22cm–24cm above the mouse for 1 min with PBS followed by 2min with 4% PFA. The trachea was tied off with a string, and the lung was removed and

placed in 4% PFA for at least 24hours at room temperature or up to one week at 4°C. Lungs were then embedded with a Leica embedding machine (EG 1150C). Paraffin blocks were kept cold and 3–4 µm sections were cut.

**Hematoxylin and Eosin (H/E)**

3–4 µm sections were deparaffinized, dipped in water and stained in Mayer's Hematoxylin solution for 1–3 min and washed under running tap water for up to 10 min. Slides were monitored under the microscope for staining progression. Slides were then incubated for 2min in Eosin dye and brought back through increasing gradients of EtOH and xylene, then coverslipped with Pertex mounting media.

**Masson's Trichrome Stain**

3–4 µm sections were deparaffinized, and stained with Gomori's Green Trichrome Stain Kit (Dako AR166) according to manufacturers protocol.

**Lung morphometry**

For alveolar morphometry, lungs were flushed with PBS at a vascular pressure of 20 cm H2O. Then PBS was infused via the trachea at a pressure of 20cm H2O and fixed with 4% paraformaldehyde in phosphate-buffered saline (pH 7.0) via the trachea at a pressure of 20 cm H2O. Investigations were performed using 5 µm sections of paraffin-embedded left lobe of the lungs. The mean linear intercept, mean air space, and mean septal wall thickness were measured after staining with hematoxylin and eosin (H/E). Total scans from the left lobe were analyzed using a Leica DM6000B microscope with an automated stage according to the procedure previously described (25, 42) which was implemented into the Qwin V3 software (Leica, Wetzlar, Germany). Horizontal lines (distance 40 µm) were placed across each lung section. The number of times the lines cross alveolar walls was calculated by multiplying the length of the horizontal lines and the number of lines per section then dividing by the number of intercepts. Bronchi and vessels above 50 µm in diameter were excluded prior to the computerized measurement. The airspace was determined as the non-parenchyma, non-stained area. The septal wall thickness was measured as the length of the line perpendicularly crossing a septum. From the respective measurements, mean values were calculated.

**Fibrosis quantification on histological sections**

Ashcroft scoring was performed blinded using a modified Ashcroft scoring protocol as described by (14) on H/E stained sections of murine left lobes. Traditionally, multiple 20X images are scored, however we imaged stained left lobes with light-microscopy at the lowest objective (1.25X), which allowed for visualization of the entire section. ImageJ software was used to measure the area of the lung that was covered in confluent fibrotic mass (data are

presented as % confluent fibrosis per total area of the section). Sections were measured blindly, a total of 3 times, and scores were averaged.

**Hydroxyproline assay**

QuickZyme total collagen assay was performed according to manufacturer's instructions. Briefly, either cranial and accessory or caudal and medial lobes were extracted, rinsed briefly in PBS and dried overnight in a ventilated hood. Lungs were weighed and 6 M HCl was added for a final concentration of 50 mg tissue per ml. Lungs and collagen standards were then incubated for 20 hours overnight at 95°C and cooled to room temperature. Next tubes were centrifuged at 13,000 x g for 10 min. Hydrolyzed supernatant was diluted 10-fold with 4 M HCl and used for the assay. A microplate reader (Tecan Infinite 200 PRO) was used for color detection. A standard curve was calculated from the collagen standards and the total hydroxyproline content was assessed.

**RNA extraction**

After lung function measurements were taken, the right bronchus was clamped and either cranial and accessory or caudal and medial lobes were removed, placed in TRIZOL, homogenized in GentleMACs and frozen in liquid nitrogen for RNA extraction. Next, transcardiac perfusion of the left lobe was performed with a 20 G needle and 15 ml PBS.

**Western blot**

Loading buffer was added to protein samples from cell extracts (5% SDS in bromophenol blue and β-mercaptoethanol) denatured for 5 min at 95°C and cooled on ice. At least 10 μg of sample was loaded on a 10% polyacrylamide gel and run at 25 mA per gel for approximately 2 hrs. Samples were then electrically transferred to a polyvinylidene fluoride (PVDF) membrane (Amersham) by semi-dry electro blotting (70 mA per Gel; gel size: 7 x 9 cm) for 90 min. The membrane was blocked with 5% milk in TBS blocking buffer at RT on shaker for 1 h followed by incubation with primary antibody: COL1a1 (Meridian #T47770R) FGF1 (Abcam #ab9588 1:2000), FGF7 (Santa Cruz #sc27126 1:200), FGF10 (Abcam #ab71794, 1:200), Col1a1 (Meridian #T40777R, 1:1000, 8% gel), SPRY2 (Santa Cruz #sc10082, 1:200), SPRY4 (Santa Cruz #sc30051, 1:200), FGFR1 (Santa Cruz #sc-121, 1:200), FGFR2 (Santa Cruz #sc-122, 1:200), p-ERK1/2 (Cell Signaling #4370S; 1:1000), total ERK1/2 (Cell Signaling #9102S; 1:1000), p-AKT total (Cell Signaling #4060S, 1:1000), total-AKT (Cell Signaling #4691S, 1:3000) ß-Actin (Abcam #ab8227; 1:30000), GAPDH (Cell Signaling #cs2118, 1:1000) overnight at 4°C. After washing with 1X TBS-T four times for 15 min each, the membrane was incubated with swine anti-Rabbit HRP (Dako #P0217) secondary antibody (dilution 1:2000) at RT for 1hr followed by four times washing with 1X TBS-T buffer for 15 min each. The protein bands were detected by ECL (Enhanced Chemi-luminescence, Amersham, Germany) treatment, followed by exposure of the membrane.

**Quantitative PCR**

RNA was reverse-transcribed (Qiagen QuantiTect Reverse Transcription Kit (205313). cDNA was diluted to a concentration between 20 ng/µl. Primers were designed using Roche Applied Sciences online Assay Design Tool. All primers were designed to span introns and blasted using NCBI software for specificity. Sybr Green Master Mix (Applied Biosciences 4309155) was used for RT-PCR with a Roche LightCycler 480 machine. Samples were run in triplicates using *Hprt* as reference genes for mouse samples.

**FACS**

Accessory and caudal lobes were isolated in ice-cold Hank's balanced salt solution (HBSS). Next, lobes were chopped finely using sterile razor blades and transferred to a 10ml solution of 0.5% collagenase in HBSS. Then, solution was heated to 37°C on a hot plate stirring on high for 60 min. Next the dissociated homogenate was passed through 18G, 20G, 24G needles respectively, then filtered through 70 µm and 40 µm filter. One volume HBSS was added to dilute collagenase and homogenates were centrifuged at 1500 rpm for 5 min to remove the enzyme solution. Cells were then resuspended in 500 µl 0.5% FCS in PBS and stained with Anti-RFP pAb Rabbit, Life Technologies, R10367 (1:200) for 20 minutes at 4°C, followed by washing and flow cytometric analysis with LSR Fortessa equipped with FACSDiva™ software (BD Bioscience).

**Statistical analyses**

One-way ANOVA was performed on densitometry plots of western blots followed by a Dunnets Test of significance. A Student's t-Test was performed on the log-transformed value of the qPCR fold changes as well as compliance, hydroxyproline, and confluent areas of fibrosis measurements. For FACS analyses, t-tests were performed on the probit values. A binomial significance test was used to determine the statistical significance of soluble Fgfr2b detection. Conformity of the data with the assumptions of the tests was checked with residual analysis.

**Results**

**Modest recruitment of the Fgf-signaling pathway during spontaneous repair initiated by bleomycin-induced lung injury in mice**

To investigate whether the endogenous Fgf-signaling pathway is recruited during bleomycin-induced lung injury, CD1 mice were given 1U/kg bleomycin intratracheally (i.t.) or saline. This

bleomycin dose generates robust fibrosis and gives a survival rate of 100% at day 28 in CD1 mice (Figure 1A). Mice were sacrificed at given time points according to weight loss to ensure maximal survival to day 28 (Figure 1B). Injury was confirmed in each mouse by lung compliance measurements (Figure 1C), calculation of confluent fibrotic areas of H/E stained left lobes (Figure 1D), hydroxyproline deposition (Figure 1E), Masson's Trichrome staining (Figure F-J), and Col1a1 western blotting of whole lung homogenate (Figure 1K, L). In this model, bleomycin-induced lung injury peaked between 14 and 21 dpi. An additional model using historical controls (5U/kg, C57bl/6 females), was also used to comparatively evaluate Fgf-signaling targets and mRNA expression and similar results were obtained (data not shown).

Next, western blots were performed on Fgfr2b ligands, receptors, and downstream signaling targets on lung homogenate lysates isolated from animals 7, 14, 21 and 28 days after bleomycin injury or 2 weeks after saline administration. Col1a1 expression was used as an indicator of fibrotic injury and most strongly expressed at 14 dpi and slightly reduced thereafter (Figure 1K, L). Fgf ligands were decreased for the most part following injury with the exception of Fgf10, which was slightly elevated compared to Fgf1 and Fgf7 at 14 dpi (Figure 1K, L). Fgfr1 and Fgfr2 expression increased significantly following injury. Importantly, qPCR analyses indicated that Fgfr11b, Fgfr2c, and Fgfr1c isoforms were increased while Fgfr2b remained decreased (Figure 1M). Spry2, a negative regulator of Mapk-signaling in the epithelium was decreased following injury, though expression was increased at 28 dpi (Figure 1K, L). Spry4, a negative regulator of Mapk-signaling in the cells of mesenchymal origin (lung fibroblasts) was slightly elevated at 21 and 28 dpi (Figure 1K, L). Etv-4, a downstream target of Fgf10 signaling, also known as Pea-3, was strongly induced following injury (Figure 1K, L). Lastly, general Mapk-signaling targets, which are also targets of Fgf-signaling were evaluated. At 7 dpi, p-Akt was slightly increased and again strongly activated at 28 dpi (Figure 1K,L). The marker p-Erk1 peaked at 14 dpi and decreased at 28 dpi (Figure 1K, L), while p-Erk2 was not significantly regulated (Figure 1K,L). Compared to mice injured with a higher dose of bleomycin (5U/kg, data not shown), p-Akt signaling was similarly regulated. It was strongly induced 3–4 weeks following injury (Figure 1K,L). In addition, p-Erk1 and p-Erk2 were moderately regulated in both models.

In summary, during spontaneous repair after bleomycin injury in wild type mice, Fgf10 expression was moderately increased along with receptor Fgfr1b, and downstream targets Spry2, Etv4, and p-Akt at 28 dpi. The endogenous, epithelial expressed Fgfr2b receptor, was drastically reduced following bleomycin-injury (Figure 1M) and began to recover expression at 21 dpi while c-isoform expression remained significantly elevated. The significance and contribution of the Fgf10/Fgfr1b-signaling axis to lung repair is still elusive and will require further investigation.

**Validation of the *Rosa26$^{rtTA/+}$;tet(O)sFgfr2b*/+ (DTG) transgenic line**

To test whether the attenuation of all Fgfr2b ligands would result in increased fibrosis, the *Rosa26$^{rtTA/+}$;tet(O)sFgfr2b*/+ ; in this study referred to as the double transgenic (DTG) mouse line was used (28) (Figure 2A). The *Rosa26* promoter drives ubiquitous expression of reverse tetracycline transactivator, which in the presence of doxycycline (dox), binds a tetracycline response sequence. Binding results in the activation of a CMV promoter, which drives expression of a chimeric transgene containing the extracellular binding domain of Fgfr2b fused with the heavy chain domain of IgG (Figure 2A). The line was previously used in the context of naphthalene and hyperoxia lung injury to demonstrate the critical role of Fgfr2b ligands in the lung repair process (12, 13, 39). In addition, this line was also used to define the role of Fgfr2b ligands during early lung embryonic and late lung development (22), limb development (5) postnatal mammary gland development (29) incisor homeostasis (28) and gut homeostasis (6).

In this study, DTG littermates lacking the *Rosa26$^{rtTA/+}$* construct (*Rosa26$^{+/+}$;tet(O)sFgfr2b/*+) were used as controls, and referred to as single transgenics or (STG). To confirm the functionality of soluble Fgfr2b in our experimental conditions, validation was also performed in adult female animals. First, the lung-specific efficiency of the driver was tested using *Rosa26$^{rtTA/+}$;tet(O)Cre/+;Tomato$^{fl/+}$* mice fed +dox-food for 7 days (Figure 2E-F). RFP expression was detected in approximately 25% of total cells by FACS and in none of the cells in mice lacking the *tet(O)Cre* transgene as illustrated by fluorescence stereomicrosopy (Figure 2B-E''').

In order to confirm the function of the chimeric receptor in adult lungs, a study was performed to test the ability of induced DTG lungs (+dox food ad libitum) to attenuate exogenous FGF7 signaling. Female STG mice were used as controls and received PBS with 0.1% BSA, the same solution in which the recombinant FGF7 was resuspended. DTG mice were fed either normal food or +dox food for one week. Next, females from each group received an intra-tracheal dose of 10 µg of rFGF7. Then, 30 minutes later, the whole lung was collected, and lysates were blotted for p-Akt and p-Erk1/2 signals. While +dox DTG mice blocked the FGF7-mediated elevation in p-Akt and p-Erk1-signals to levels of PBS-treated controls, p-Erk2 remained elevated. Failure to block p-Erk2 was possibly due to overabundance of FGF7 and resultant signaling via endogenous Fgfr2 receptors (Figure 2F–H').

Morphometric analyses were performed on STG and DTG mice fed +dox food from PN1 to PN105 (Figure 2I-L). The chimeric transcript was detected only in DTG mice (Figure 2I) and lung compliance remained unaffected (Figure 2J). In concurrence with previous studies (12), morphometric analyses revealed no significant differences in mean linear intercept, airspace, or septal wall thickness in DTG mice (Figure 2K-M). While no lung defects were present, DTG

mice fed +dox food from postnatal days (PN) 28-88 showed characteristic inhibition of maxillary incisor regeneration (Figure 4H-H') (5).

**Attenuation of *Fgfr2b* ligands during fibrosis formation post-bleomycin injury did not result in increased fibrosis**

To determine whether endogenous Fgfr2b ligands expedite fibrosis resolution, a relatively low dose of bleomycin (1U/kg i.t.), which generated between 80% and 100% survival and mild fibrosis at day 28 was used. First, Fgfr2b ligands were attenuated from (d6-d14) (Figure 3) and next during fibrotic resolution (d14-d28) (Figure 4). Fgfr2b ligands attenuation had no impact on relative survival (Figure 3A) though a trend towards delayed weight recovery in DTG mice was observed (Figure 3B). Specific soluble *Fgfr2b* expression in DTG was confirmed (Figure 3C). A slight increase in lung compliance was measured at day 28 in DTG vs. STG (Figure 3D). Upon histological examination both STG and DTG lungs showed areas of fibrosis (Figure 3E-F). However, quantification of the confluent areas of fibrosis in the left lobe did not reveal any difference between DTG and STG (Figure 3G). In agreement with these results, no differences were observed for total hydroxyproline (Figure 3H). Together, these results indicate that attenuation of Fgfr2b ligands post bleomycin injury (d6-d28) had no impact on fibrosis resolution by 28 dpi.

Although downstream targets were just moderately engaged in wild type mice injured with either 1.0U/kg or 5.0U/kg bleomycin doses, a slightly higher bleomycin dose was performed (2U/kg i.t.) in order to test whether endogenous Fgfr2b ligands would play an important role in lung repair following more severe injury. To focus on the contribution of Fgfr2b ligands to the resolution phase, ligands were attenuated from 14 through 28 dpi. No difference in survival rate (Figure 4A) was observed. The relative weight change between DTG and STG were similar (Figure 4B). The expression of soluble *Fgfr2b* was detected only in DTG as previously reported (Figure 4C). No difference in lung function was observed (Figure 4D). However, no difference was observed for hydroxyproline deposition between DTG and STG (Figure 4H) was observed. In summary, attenuation of Fgfr2b ligands post bleomycin injury following the peak of fibrosis (d14-d28) does not have any impact on the extent of fibrosis at day 28.

**Attenuation of *Fgfr2b* ligands immediately following bleomycin injury did not result in increased fibrosis**

Attenuating Fgfr2b ligands at later stages following injury (d6-d28 and d14-d28) had no effect on the level of bleomycin induced lung injury incurred. As Fgfr2b ligands are known to have a protective effect on lung epithelium, next, it was tested whether attenuation of endogenous Fgfr2b ligands signaling immediately afterwards and throughout injury impacts the extent of fibrosis incurred at 28 dpi. Fgfr2b ligands were attenuated throughout injury (d0–d28). With the exception of one STG animal, all animals survived until sacrificed at day 28 (Figure 5A). No significant differences in relative weight change were observed, although as in Figure 5B,

a trend towards delayed weight recovery in DTG mice was observed (Figure 5B). Specific soluble *Fgfr2b* expression in DTG was confirmed (Figure 5C). No significant change in lung compliance was measured at day 28 in DTG vs. STG (Figure 5D). Upon histological examination both STG and DTG had areas of fibrosis (Figure 5E-F). However, quantification of the confluent fibrosis areas did not reveal any difference between DTG and STG lungs (Figure 5G). In agreement with these results, no differences were observed for total hydroxyproline (Figure 5H). Attenuation of Fgfr2b ligands in DTG mice for the duration of the injury did not lessen fibrosis incurred at 28 dpi.

In an attempt to further engage endogenous repair mechanisms, 3.0U/kg i.t of bleomycin was used in the final experiment (Figure 6). The soluble receptor was induced from the day of bleomycin-injury until the day of sacrifice; between 6 and 11 dpi (Figure 6). While the initial aim of this study was to analyze the extent of fibrosis at 28 dpi, 3.0U/kg i.t of bleomycin was too severe for CD1 mice. Therefore mice were sacrificed and analyzed at earlier time points. 5 mice from both the STG and the DTG groups were removed at day 6 for analyses based on weight-loss criteria (< 20% of initial weight, data not shown). The other mice (STG; n=3 and DTG; n=4) were analyzed at day 11. Induction of the soluble receptor was detected in DTG mice (Figure 6A). A trend towards increased weight loss for DTG mice that survived to day 11 was observed (Figure 6B). While some variability in measurements occurred due to differences in the day of sacrifice (d6-d11), no differences between STGs and DTGs were detected at any time point in regards to compliance (Figure 6C), hydroxyproline (Figure 6D) and the confluent fibrotic areas (Figure 6G). In wild type mice, bleomycin injury triggered decreased *Sftpc* expression at day 7 and *Scgb1a1* at day 14, (data not shown). Therefore, expression of AECII cell specific transcript *Sftpc*, *Scgb1a1* for Clara cells, and the general epithelial marker *EpCam* were measured in animals sacrificed at 6 dpi. However, no differences in marker expression were observed between DTG and STG lungs (Figure 6H–J).

## Discussion

### Fgfr2b ligand signaling is important for lung development and repair

Fgfs play pleiotropic roles both during organogenesis and homestasis (15). Fgfr2b ligands are part of a family of 22 identified members. Fgf10 is required for lung formation and loss of *Fgf10* leads to lung agenesis while loss of *Fgf1* and *Fgf7* during development does not result in a lung phenotype in mice. The cellular and molecular basis for differences between Fgf7 and Fgf10 signaling are still unclear. Recently, mass spectometry-based proteomics revealed that Fgf7 and Fgf10 elicit distinct biochemical response downstream of the Fgfr2b receptor. In particular, Fgf7 leads to rapid but transient phosphorylation of Akt and Shc while Fgf10 leads to the progressive and sustained phosphorylation of these mediators. In addition, Fgf10

triggers phosphorylation of tyrosine 734 and the associated recruitment of SH3bp4, a relatively novel adaptor protein. It has been proposed that Fgf10 leads to increased recycling of Fgfr2b at the cell surface while Fgf7 results in transient signaling (8). Unlike Fgf7 and Fgf10, Fgf1, not only signals via Fgfr2b, but via all Fgf receptor isoforms.

Fgf10 appears to be not only critical for the survival and proliferation of the distal epithelial lung progenitors (35) but also for the repair of the bronchiolar epithelium following naphthalene exposure (39). Lung epithelial cell specific overexpression of *Fgf10* in mice during the first, second or third week post-bleomycin injury was both protective and therapeutic as characterized by increased survival and attenuated lung fibrosis (11). Administration of Fgf7 or Palifermin, a pharmacological agent composed of a truncated form of Fgf7, also reduced fibrosis and increased survival both in both rats and mice (7, 10, 22, 32). In humans, haploinsufficiency for *FGF10* is associated with COPD (18). Likewise, in humans, SNPs in *FGF7* correlate with increased risk for developing COPD (4).

In contrast to previous studies which used used exogenous Fgfr2b ligands to attenuate bleomycin-induced lung injury, this study first assessed the activation of endogenous Fgfr2b ligands in injured wild type mice, and then attenuated Fgfr2b ligands following bleomycin injury in order to assess their contribution to lung repair. Given the significant reduction in Fgfr2b receptor expression following bleomycin injury, it was not surprising that attenuation of endogenous Fgfr2b ligands had no effect on fibrosis outcome.

**DTG mice efficiently attenuate endogenous Fgfr2b ligands**

The *Rosa26$^{rtTA/+;}$tet(O)sFgfr2b/+* (DTG) mouse line was used to ubiquitously trap all Fgfr2b-ligands during injury. Fgf1, in addition to ligands of the Fgf7 subfamily: Fgf3, Fgf7, Fgf10, and Fgf22, bind most strongly to Fgfr2b (43). Though Fgf10 contains a nuclear localization signal and may in some contexts act in an intracrine fashion (20), the *Rosa26$^{rtTA/+}$; tet(o)sFgfr2b/+* model has been demonstrated to mimic the loss of *Fgf10* expression during development (35) demonstrating that Fgf10's activity in the lung is mainly via secreted, paracrine signaling. The impact of trapping Fgfr2b ligands during lung injury has been previously reported. Induction of soluble Fgfr2b under the *SpC-rtTA/+* promoter in adult mice subjected to hyperoxia injury led to abnormal expression of surfactant during injury which contributed to increased lethality (12). A similar result was obtained using *Rosa26$^{rtTA/+}$;tet(o)sFgfr2b/+* neonates exposed to hyperoxia (Chao and Bellusci, unpublished results). Furthermore, in the context of naphthalene injury (39) as well as H1N1 influenza virus infection (Quantius et. al., manuscript in preparation) lung injury was increased in DTG animals. Mice used in this study were thoroughly validated and demonstrated both the embryonic and adult phenotypes characteristic of this line.

**Attenuation of endogenous Fgfr2b ligands during bleomycin-injury did not result in increased fibrosis**

Doxycycline fed bleomycin-injured *Rosa26$^{rtTA/+}$;tet(o)sFgfr2b/+* (DTG) mice did not incur increased fibrosis compared to injured STG mice. There are several explanations for the lack of increased injury in DTG mice following bleomycin injury. First, the weak recruitment of Fgf ligands in this injury model indicated an insignificant contribution of endogenous Fgfr2b-ligands to the repair process. Second, while solFgfr2b traps both Fgf7 and Fgf10 ligands, which have been shown to convey protective signals to the injured epithelium, it also traps Fgf1, which binds to all Fgfrs. Though its effects are not well characterized, Fgf1-signaling is potentially ambivalent in the context of bleomycin lung injury. As Fgf1 signals to cells of both epithelial and mesenchymal origins, blocking an Fgf1-mediated survival signal to fibroblasts following bleomycin injury, especially following 14 dpi, when fibroblasts are most abundant, may be beneficial. Moreover, in a study using a soluble, dominant negative Fgfr2c-isoform construct, it was demonstrated that blocking mesenchymal Fgfr2c mediated signaling following bleomycin injury attenuated fibrosis (17). Third, although FACS analyses of *Rosa26$^{rtTA/+}$;Tomato$^{fl/+}$* mice revealed that doxycycline induced *rtTA* expression in 25% of the lung cells, for maximal ligand attenuation during bleomycin injury, a lung specific driver may be required. Lastly, compensation by other endogenous repair pathways such as Wnt (37), may adequately compensate for the attenuation of Fgf-signaling. In the future, lung cell type specific models targeting specific ligands and receptors are needed to more accurately dissect the role of Fgf-signaling in lung repair.

**Tyrosine kinase inhibitors demonstrate therapeutic effects in bleomycin-treated mice further suggesting endogenous Fgfr2b ligand signaling is dispensable for repair**

Tyrosine kinase receptors mediate a variety of growth factor signaling pathways. High levels of MAPK and ERK phosphorylation are associated with IPF. Three major tyrosine kinase pathways relevant for lung disease have been described: the VEGFR and PDGFR and the FGFR pathways. The tyrosine kinase inhibitor BIBF1120 blocks these pathways and demonstrated a protective and therapeutic in the bleomycin model (40). In addition, phase III clinical trials demonstrated that BIBF1120 treatment both decreased the rate of decline in forced vital capacity and reduced the number of acute exacerbations in IPF patients (41). In mouse models, just as enhanced activation of the epithelial receptor tyrosine kinase Fgfr2b-isoform via exogenous Fgfr2b ligands leads to epithelial protection and lessens fibrosis, attenuation of Fgfr2c-isoform signaling also attenuates fibrosis. These results suggest that enhanced Fgfr2b-isoform signaling expedites lung protection and repair, while Fgfr2c-isoform ligand signaling (via Fgf1, Fgf2, Fgf9) may fuel the fibrosis fire by relaying survival signals to fibroblasts. In conclusion, although global tyrosine kinase inhibitors such as BIBF1120 likely inhibit FGFR2b-signaling, the contribution of VEGF, PDGF, and FGFR2(c) to fibrosis formation may be far greater. Whether exogenously stimulating Fgfr2b-signaling following

treatment with tyrosine kinase inhibitors further attenuates bleomycin-induced fibrosis injury remains to be investigated.

**Acknowledgements**

We would like to thank Jonathan Branch, Clarence Wigfall, and Soula Danopolous for their technical support at CHLA. AAR and SB acknowldege the support of the Russian Government Program of Competitive growth of Kazan Federal University.

**References**

1. **Antoniu SA**. Nintedanib (BIBF 1120) for IPF: a tomorrow therapy? *Multidiscip Respir Med* 7: 41, 2012.
2. **Bellusci S, Grindley J, Emoto H, Itoh N, Hogan B**. Fibroblast growth factor 10 (FGF10) and branching morphogenesis in the embryonic mouse lung [Online]. *Development* 124: 4867–4878, 1997. http://dev.biologists.org/content/124/23/4867.abstract?ijkey=9bab527d4f955e41d0a7ebcc3c868d143209da1a&keytype2=tf_ipsecsha [5 Jul. 2013].
3. **Belteki G, Haigh J, Kabacs N, Haigh K, Sison K, Costantini F, Whitsett J, Quaggin SE, Nagy A**. Conditional and inducible transgene expression in mice through the combinatorial use of Cre-mediated recombination and tetracycline induction. *Nucleic Acids Res* 33: e51, 2005.
4. **Brehm JM, Hagiwara K, Tesfaigzi Y, Bruse S, Mariani TJ, Bhattacharya S, Boutaoui N, Ziniti JP, Soto-Quiros ME, Avila L, Cho MH, Himes B, Litonjua AA, Jacobson F, Bakke P, Gulsvik A, Anderson WH, Lomas DA, Forno E, Datta S, Silverman EK, Celedón JC**. Identification of FGF7 as a novel susceptibility locus for chronic obstructive pulmonary disease. *Thorax* 66: 1085–90, 2011.
5. **Danopoulos S, Parsa S, Al Alam D, Tabatabai R, Baptista S, Tiozzo C, Carraro G, Wheeler M, Barreto G, Braun T, Li X, Hajihosseini MK, Bellusci S**. Transient Inhibition of FGFR2b-ligands signaling leads to irreversible loss of cellular β-catenin organization and signaling in AER during mouse limb development. *PLoS One* 8: e76248, 2013.
6. **Denise Al Alam, Soula Danopoulos, Frederic G Sala, Dana Almohazey, G. Esteban Fernandez, Mark R Frey, Henri R Ford, Tracy Grikscheit SB**. Fgf10 alters the balance between Goblet cells and Paneth cells in the adult mouse small intestine. *Am. J. Physiol. - Gastrointest. Liver Physiol. in press*.
7. **Deterding RR, Havill AM, Yano T, Middleton SC, Jacoby CR, Shannon JM, Simonet WS, Mason RJ**. Prevention of bleomycin-induced lung injury in rats by keratinocyte growth factor. [Online]. *Proc Assoc Am Physicians* 109: 254–68, 1997. http://www.ncbi.nlm.nih.gov/pubmed/9154642 [10 Mar. 2013].
8. **Francavilla C, Rigbolt KTG, Emdal KB, Carraro G, Vernet E, Bekker-Jensen DB, Streicher W, Wikström M, Sundström M, Bellusci S, Cavallaro U, Blagoev B, Olsen J V**. Functional proteomics defines the molecular switch underlying FGF receptor trafficking and cellular outputs. *Mol Cell* 51: 707–22, 2013.
9. **Gossen M, Bujard H**. Tight control of gene expression in mammalian cells by tetracycline-responsive promoters. [Online]. *Proc Natl Acad Sci U S A* 89: 5547–51, 1992.

http://www.pubmedcentral.nih.gov/articlerender.fcgi?artid=49329&tool=pmcentrez&rendertype=abstract.

10. **Guo J, Yi ES, Havill AM, Sarosi I, Whitcomb L, Yin S, Middleton SC, Piguet P, Ulich TR**. Intravenous keratinocyte growth factor protects against experimental pulmonary injury. [Online]. *Am J Physiol* 275: L800–5, 1998. http://www.ncbi.nlm.nih.gov/pubmed/9755113 [14 May 2013].
11. **Gupte V V, Ramasamy SK, Reddy R, Lee J, Weinreb PH, Violette SM, Guenther A, Warburton D, Driscoll B, Minoo P, Bellusci S**. Overexpression of fibroblast growth factor-10 during both inflammatory and fibrotic phases attenuates bleomycin-induced pulmonary fibrosis in mice. *Am J Respir Crit Care Med* 180: 424–36, 2009.
12. **Hokuto I, Perl A-KT, Whitsett JA**. Prenatal, but not postnatal, inhibition of fibroblast growth factor receptor signaling causes emphysema. *J Biol Chem* 278: 415–21, 2003.
13. **Hokuto I, Perl A-KT, Whitsett JA**. FGF signaling is required for pulmonary homeostasis following hyperoxia. *Am J Physiol Lung Cell Mol Physiol* 286: L580–7, 2004.
14. **Hübner R-H, Gitter W, El Mokhtari NE, Mathiak M, Both M, Bolte H, Freitag-Wolf S, Bewig B**. Standardized quantification of pulmonary fibrosis in histological samples. *Biotechniques* 44: 507–11, 514–7, 2008.
15. **Itoh N, Ornitz DM**. Fibroblast growth factors: from molecular evolution to roles in development, metabolism and disease. *J Biochem* 149: 121–30, 2011.
16. **Izvolsky KI, Shoykhet D, Yang Y, Yu Q, Nugent MA, Cardoso W V**. Heparan sulfate-FGF10 interactions during lung morphogenesis. [Online]. *Dev Biol* 258: 185–200, 2003. http://www.ncbi.nlm.nih.gov/pubmed/12781692 [7 Jul. 2013].
17. **Ju W, Zhihong Y, Zhiyou Z, Qin H, Dingding W, Li S, Baowei Z, Xing W, Ying H, An H**. Inhibition of α-SMA by the ectodomain of FGFR2c attenuates lung fibrosis. *Mol Med* 18: 992–1002, 2012.
18. **Klar J, Blomstrand P, Brunmark C, Badhai J, Håkansson HF, Brange CS, Bergendal B, Dahl N**. Fibroblast growth factor 10 haploinsufficiency causes chronic obstructive pulmonary disease. *J Med Genet* 48: 705–9, 2011.
19. **Korfei M, Ruppert C, Mahavadi P, Henneke I, Markart P, Koch M, Lang G, Fink L, Bohle R-M, Seeger W, Weaver TE, Guenther A**. Epithelial endoplasmic reticulum stress and apoptosis in sporadic idiopathic pulmonary fibrosis. *Am J Respir Crit Care Med* 178: 838–46, 2008.
20. **Kosman J, Carmean N, Leaf EM, Dyamenahalli K, Bassuk JA**. Translocation of fibroblast growth factor-10 and its receptor into nuclei of human urothelial cells. *J Cell Biochem* 102: 769–85, 2007.
21. **Lewis D, Scullion J**. Palliative and end-of-life care for patients with idiopathic pulmonary fibrosis: challenges and dilemmas. [Online]. *Int J Palliat Nurs* 18: 331–7, 2012. http://www.ncbi.nlm.nih.gov/pubmed/22885965 [10 Mar. 2013].
22. **Liu C-J, Ha X-Q, Jiang J-J, Lv T-D, Wu C**. Keratinocyte growth factor (KGF) gene therapy mediated by an attenuated form of Salmonella typhimurium ameliorates radiation induced pulmonary injury in rats. [Online]. *J Radiat*

*Res* 52: 176–84, 2011. http://www.ncbi.nlm.nih.gov/pubmed/21436609 [26 Mar. 2013].

23. **Lü J, Izvolsky KI, Qian J, Cardoso W V**. Identification of FGF10 targets in the embryonic lung epithelium during bud morphogenesis. *J Biol Chem* 280: 4834–41, 2005.
24. **Madisen L, Zwingman TA, Sunkin SM, Oh SW, Zariwala HA, Gu H, Ng LL, Palmiter RD, Hawrylycz MJ, Jones AR, Lein ES, Zeng H**. A robust and high-throughput Cre reporting and characterization system for the whole mouse brain. *Nat Neurosci* 13: 133–40, 2010.
25. **McGrath-Morrow SA, Cho C, Soutiere S, Mitzner W, Tuder R**. The effect of neonatal hyperoxia on the lung of p21Waf1/Cip1/Sdi1-deficient mice. *Am J Respir Cell Mol Biol* 30: 635–40, 2004.
26. **Nelson WJ, Nusse R**. Convergence of Wnt, beta-catenin, and cadherin pathways. *Science* 303: 1483–7, 2004.
27. **Ohuchi H, Hori Y, Yamasaki M, Harada H, Sekine K, Kato S, Itoh N**. FGF10 acts as a major ligand for FGF receptor 2 IIIb in mouse multi-organ development. *Biochem Biophys Res Commun* 277: 643–9, 2000.
28. **Parsa S, Kuremoto K-I, Seidel K, Tabatabai R, Mackenzie B, Yamaza T, Akiyama K, Branch J, Koh CJ, Al Alam D, Klein OD, Bellusci S**. Signaling by FGFR2b controls the regenerative capacity of adult mouse incisors. *Development* 137: 3743–52, 2010.
29. **Parsa S, Ramasamy SK, De Langhe S, Gupte V V, Haigh JJ, Medina D, Bellusci S**. Terminal end bud maintenance in mammary gland is dependent upon FGFR2b signaling. *Dev Biol* 317: 121–31, 2008.
30. **Perl A-KT, Tichelaar JW, Whitsett JA**. Conditional gene expression in the respiratory epithelium of the mouse. [Online]. *Transgenic Res* 11: 21–9, 2002. http://www.ncbi.nlm.nih.gov/pubmed/11874100 [8 Oct. 2014].
31. **Rafii R, Juarez MM, Albertson TE, Chan AL**. A review of current and novel therapies for idiopathic pulmonary fibrosis [Online]. *J. Thorac. Dis.* 5: 48–73, [date unknown]. http://www.jthoracdis.com/article/view/843/html [15 May 2014].
32. **Sakamoto S, Yazawa T, Baba Y, Sato H, Kanegae Y, Hirai T, Saito I, Goto T, Kurahashi K**. Keratinocyte growth factor gene transduction ameliorates pulmonary fibrosis induced by bleomycin in mice. *Am J Respir Cell Mol Biol* 45: 489–97, 2011.
33. **Sauer B**. Inducible gene targeting in mice using the Cre/lox system. *Methods* 14: 381–92, 1998.
34. **Schwenk F, Baron U, Rajewsky K**. A cre-transgenic mouse strain for the ubiquitous deletion of loxP-flanked gene segments including deletion in germ cells. [Online]. *Nucleic Acids Res* 23: 5080–1, 1995. http://www.pubmedcentral.nih.gov/articlerender.fcgi?artid=307516&tool=pmcentrez&rendertype=abstract [8 May 2013].
35. **Sekine K, Ohuchi H, Fujiwara M, Yamasaki M, Yoshizawa T, Sato T, Yagishita N, Matsui D, Koga Y, Itoh N, Kato S**. Fgf10 is essential for limb and lung formation. *Nat Genet* 21: 138–41, 1999.
36. **Sugahara K, Iyama K, Kuroda MJ, Sano K**. Double intratracheal instillation of keratinocyte growth factor prevents bleomycin-induced lung fibrosis in rats. *J Pathol* 186: 90–8, 1998.

37. **Tanjore H, Degryse AL, Crossno PF, Xu XC, McConaha ME, Jones BR, Polosukhin V V, Bryant AJ, Cheng D-S, Newcomb DC, McMahon FB, Gleaves LA, Blackwell TS, Lawson WE**. β-catenin in the alveolar epithelium protects from lung fibrosis after intratracheal bleomycin. *Am J Respir Crit Care Med* 187: 630–9, 2013.
38. **Verkaar F, Zaman GJR**. New avenues to target Wnt/β-catenin signaling. *Drug Discov Today* 16: 35–41, 2011.
39. **Volckaert T, Dill E, Campbell A, Tiozzo C, Majka S, Bellusci S, De Langhe SP**. Parabronchial smooth muscle constitutes an airway epithelial stem cell niche in the mouse lung after injury. *J Clin Invest* 121: 4409–19, 2011.
40. **Wollin L, Maillet I, Quesniaux V, Holweg A, Ryffel B**. Anti-fibrotic and anti-inflammatory activity of the tyrosine kinase inhibitor, nintedanib, in experimental models of lung fibrosis. *J. Pharmacol. Exp. Ther.* ( February 20, 2014). doi: 10.1124/jpet.113.208223.
41. **Woodcock H V, Molyneaux PL, Maher TM**. Reducing lung function decline in patients with idiopathic pulmonary fibrosis: potential of nintedanib. *Drug Des Devel Ther* 7: 503–10, 2013.
42. **Woyda K, Koebrich S, Reiss I, Rudloff S, Pullamsetti SS, Rühlmann A, Weissmann N, Ghofrani HA, Günther A, Seeger W, Grimminger F, Morty RE, Schermuly RT**. Inhibition of phosphodiesterase 4 enhances lung alveolarisation in neonatal mice exposed to hyperoxia. *Eur Respir J* 33: 861–70, 2009.
43. **Zhang X, Ibrahimi OA, Olsen SK, Umemori H, Mohammadi M, Ornitz DM**. Receptor specificity of the fibroblast growth factor family. The complete mammalian FGF family. *J Biol Chem* 281: 15694–700, 2006.

## Figure Legends

**Figure 1: Fibrosis injury (1U/kg) peaked between 14 and 21 dpi in CD1 female, wild type mice, moderate recruitment of Fgfr2b-signaling following injury (Fgfs)**

Survival curve (**A**). Relative weight change (**B**). Compliance (**C**). Quantification of confluent fibrotic areas in H/E stains of left lobes (**D**). Hydroxyproline content of medial lobes (**E**). Massons trichrome stain of representative time points following injury (**F**-**J**) Western blots for Fgf-signaling pathway members of saline or bleomycin treated mice (**K**) Quantification of blot densities normalized to saline controls (gene of interest divided by control gene) and represented as percent of saline expression (**L**). Since the western blot antibodies used do not distinguish between receptor isoforms, qPCR was performed on epithelial (b-isoforms) and mesenchymal c-isoforms of Fgfr1 and Fgfr2 receptor. Already at 7 dpi, *Fgfr2b* was significantly reduced, and remained so until 21 dpi. At 14 dpi, c-isoforms of both receptors were increased, as well as Fgfr1b. C-isoforms remained elevated at 21 dpi, while *Fgfr1b* returned to saline levels (**M**). One-way ANOVA was performed against control values and error bars represent 95% confidence intervals; § ($p<0.05$) †($p<0.005$) ★($p<0.0001$). Scale bars: 100 μm.

**Figure 2. Validation of *Rosa26$^{rtTA/+}$;tet(O)sFgfr2b/+* (DTG) mice**

The *Rosa26* promoter drives ubiquitous expression of reverse tetracycline transactivator (rtTA), which in the presence of doxycycline (dox), binds a tetracycline response sequence. Binding results in the activation of a CMV promoter, which drives expression of a chimeric transgene containing the extracellular binding domain of Fgfr2b fused with the heavy chain domain of IgG (**A**). Lung-specific efficiency of *Rosa26* promoter was tested using *Rosa26$^{rtTA/+}$;tet(O)Cre/+;Tomato$^{fl/+}$* mice fed +dox-food for 7 days (**B**-**C**). RFP expression was detected in approximately 25% of total cells by FACS and in none of the cells in mice lacking the *tet(O)Cre* transgene as illustrated by fluorescence stereomicrosopy (**D**-**E''**). STG mice (n=3) received 50ul of PBS with 0.1% BSA, DTG mice fed normal food (n=3) or +dox food (n=4) for 1 week and were given an intra-tracheal dose of 10 μg of FGF7. 30 minutes later, the lysates were collected and blotted for p-Akt and p-Erk1/2 signals (**F**). +dox DTG mice blocked FGF7-mediated p-Akt (**G**) and p-Erk1-signals (**H**), p-ERK2 (**H'**) remained elevated, (Figure 2F–H'). The chimeric transcript was detected only in DTG mice (**I**) and lung compliance was not changed in DTG mice fed +dox food from post-natal (PN) PN1 to PN105 (**J**). Morphometric analyses were performed on these mice and (**K**-**O**) and in concurrence with previous studies no significant differences in mean linear intercept, airspace, or septal wall thickness were observed in DTG mice. Adult DTG mice fed +dox food from postnatal day (PN28-88) failed to regenerate maxillary incisors (**H**-**H'**).

**Figure 3: Lack of endogenous *Fgfr2b* ligands signaling during injury (6–28 dpi) did not lead to increased bleomycin-induced lung injury (28 dpi).**

Survival curve (**A**). Relative weight change (**B**). All DTG mice tested positive for *solFgfr2b* transcript at 28 dpi (**C**). Compliance (**D**). Low and high magnification of H/E staining of STG control mice (**E** and **E'**) and DTGs fed doxycycline food from 6 to 28 dpi (**F** and **F'**). Quantification of confluent fibrotic areas in H/E stains of left lobes (**G**). Hydroxyproline content of accessory and medial lobes (**H**). Scale bars **E** and **F**: 2 mm; **E'** and **F'**: 200 μm.

**Figure 4: Lack of endogenous *Fgfr2b* ligands signaling during injury (14–28 dpi) did not lead to increased bleomycin-induced lung injury (28 dpi).**

Survival curve (**A**). Relative weight change (**B**). All DTG mice tested positive for *solFgfr2b* transcript at 28 dpi (**C**). Compliance (**D**). Low and high magnification of H/E staining of STG control mice (**E** and **E'**) and DTGs fed doxycycline food from 14 to 28 dpi (**F** and **F'**). Quantification of confluent fibrotic areas in H/E stains of left lobes (**G**). Hydroxyproline content of accessory and medial lobes (**H**). *Col1a1* expression (**I**). Scale bars E and F: 2 mm; E' and F': 200 μm.

**Figure 5: Lack of endogenous *Fgfr2b* ligands signaling during injury (0–28 dpi) did not lead to increased bleomycin-induced lung injury (28 dpi).**

Survival curve (**A**). Relative weight change (**B**). All DTG mice tested positive for *solFgfr2b* transcript at 28 dpi (**C**). Compliance (**D**). Low and high magnification of H/E staining of STG control mice (**E** and **E'**) and DTGs fed doxycycline food from 0 to 28 dpi (**F** and **F'**). Quantification of confluent fibrotic areas in H/E stains of left lobes (**G**). Hydroxyproline content of accessory and medial lobes (**H**). Scale bars **E** and **F**: 2 mm; **E'** and **F'**: 200 μm.

**Figure 6: Lack of endogenous *Fgfr2b* ligands signaling during injury (6–11 dpi) did not lead to increased bleomycin-induced lung injury (6-11 dpi).**

All DTG mice tested positive for *solFgfr2b* transcript at 28 dpi (**A**). Relative weight change in mice that survived until 11 dpi (3/8 STG) and (4/9 DTG) (**B**). Compliance (**C**). Hydroxyproline content of accessory and medial lobes (**D**). Low and high magnification of H/E staining of STG control mice at 11 dpi (**E** and **E'**) and DTGs fed doxycycline food from 0 to 11 dpi (**F** and **F'**). Quantification of confluent fibrotic areas in H/E stains of left lobes (**G**). No decreases in epithelial marker expression were detected in injured 6 dpi DTG mice vs. STG; qPCR for *Sftpc*, *Scgb1a1*, *EpCam*; corresponding saline controls normalized to one (data not shown) (**H**–**J**). Scale bars **E** and **F**: 2 mm; **E'** and **F'**: 200 μm.

MacKenzie et. al, AJP Lung Figure 1

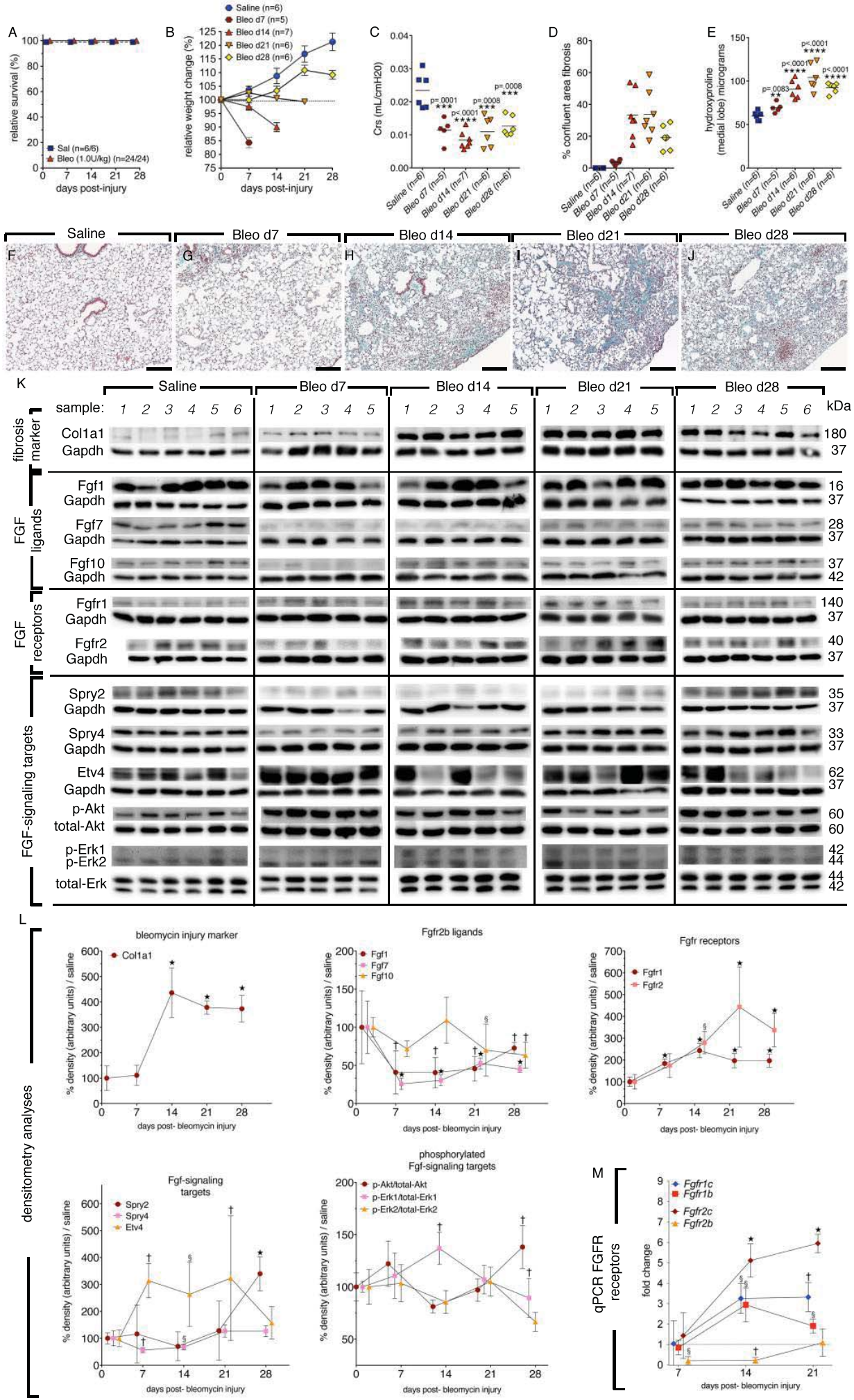

MacKenzie et. al, AJP Lung Figure 2

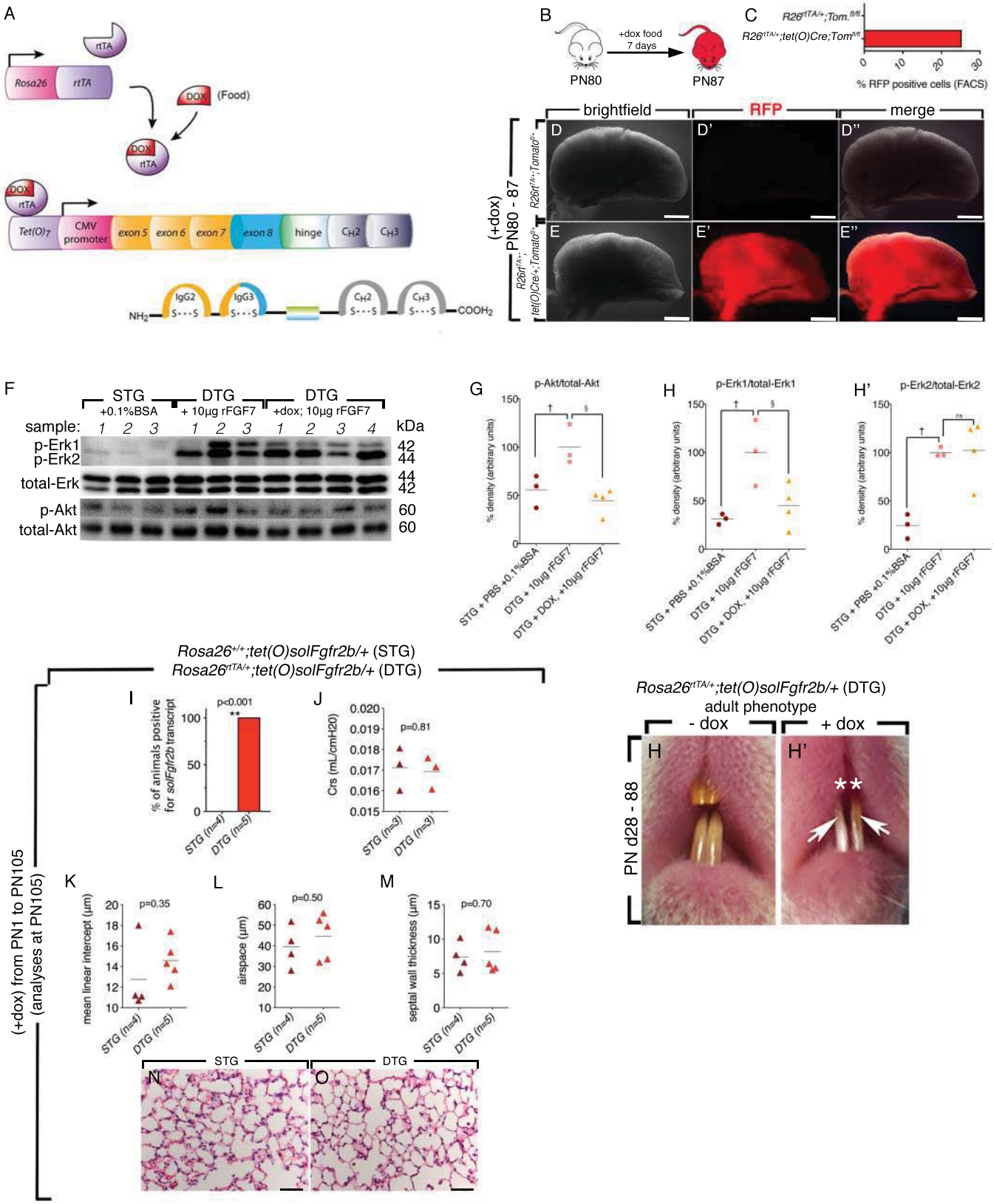

MacKenzie et. al, AJP Lung Figure 3

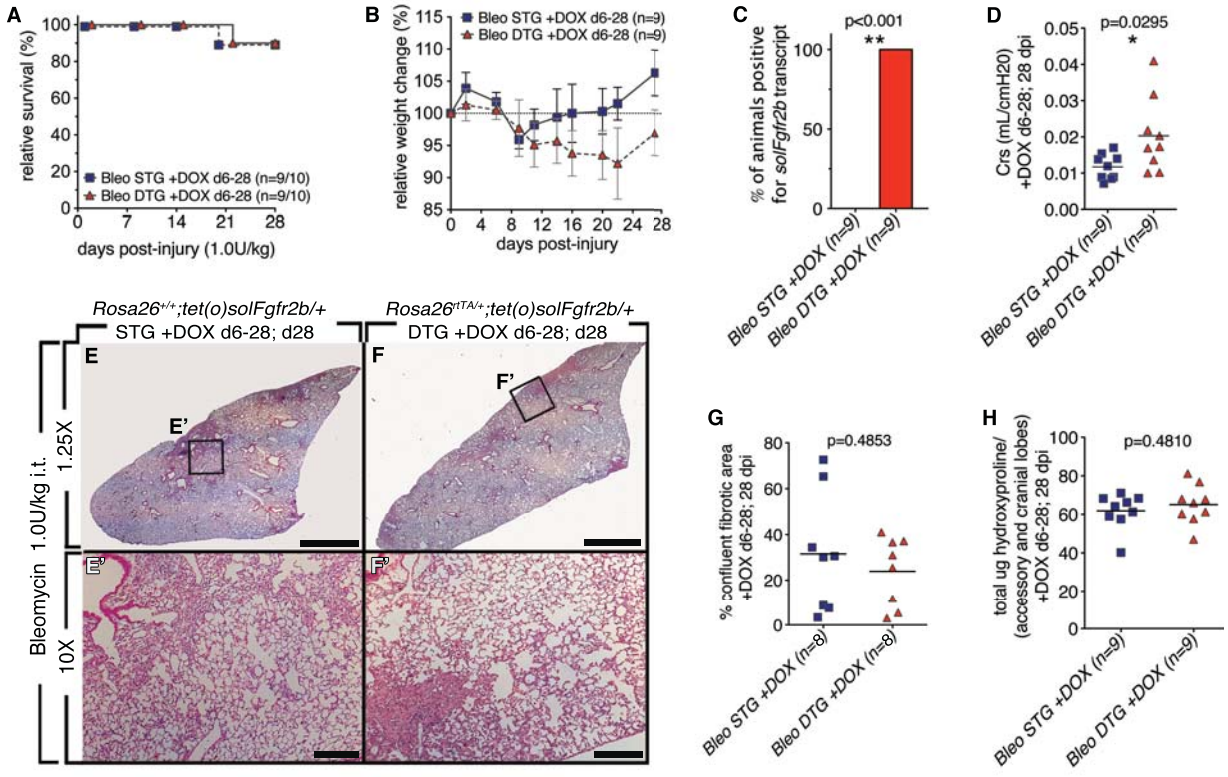

MacKenzie et. al, AJP Lung Figure 4

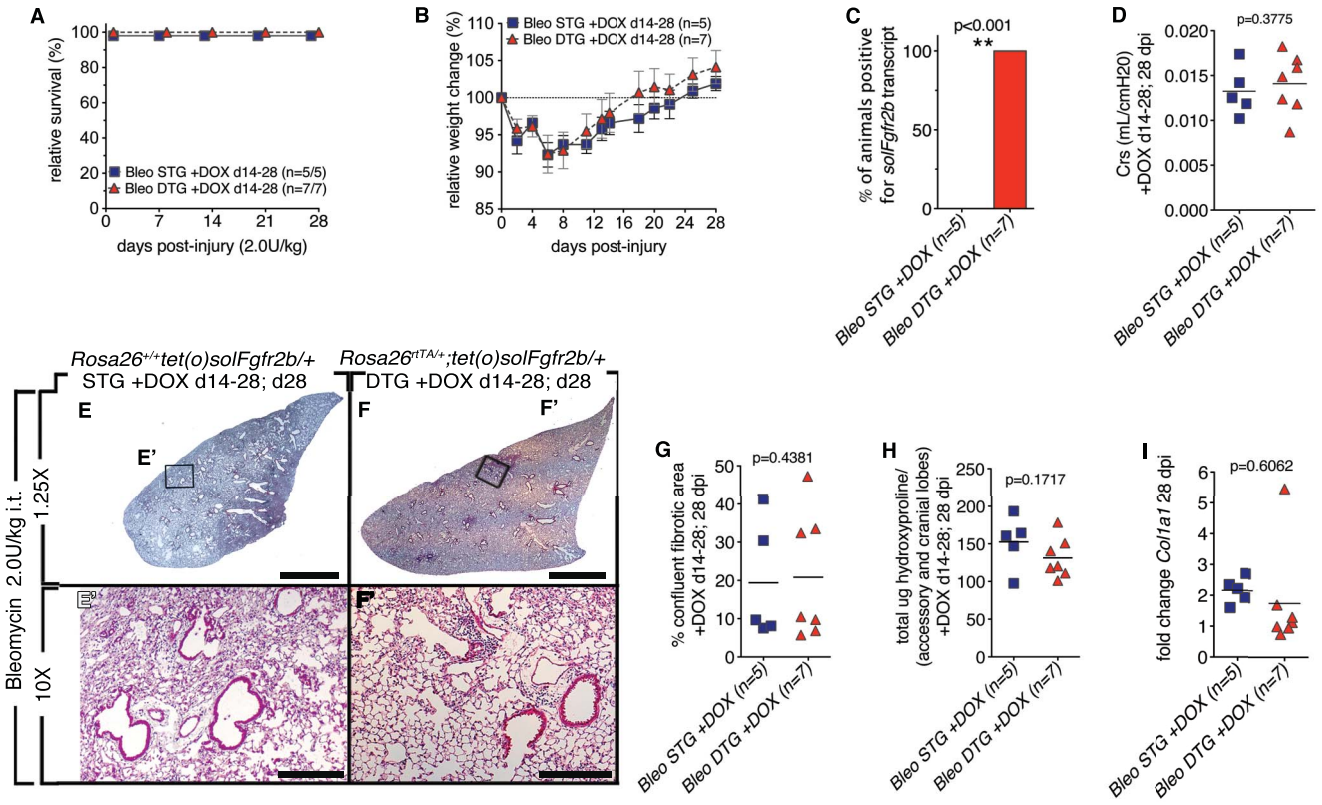

MacKenzie et. al, AJP Lung Figure 5

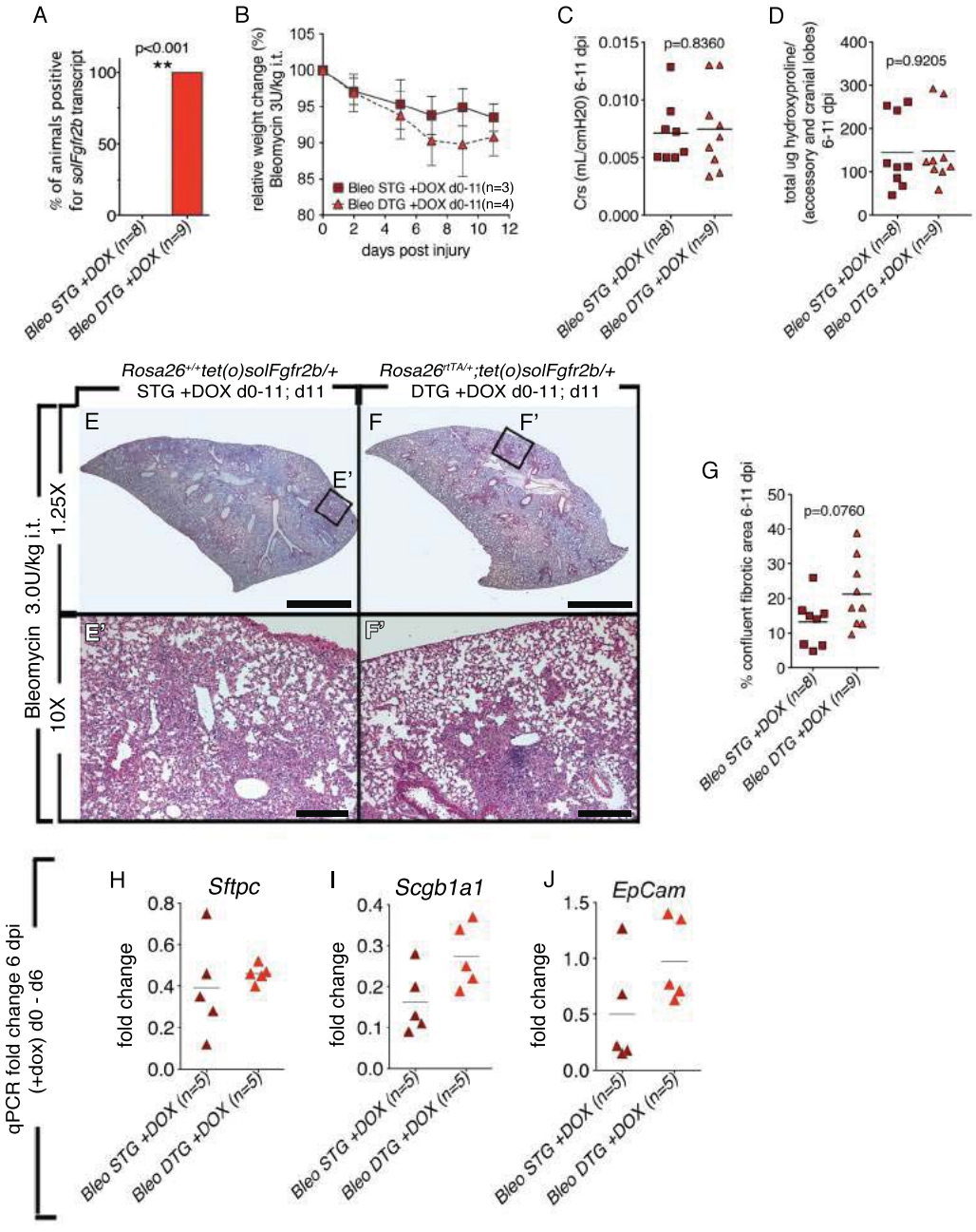

MacKenzie et. al, AJP Lung Figure 6